Article:
Racki, G, Rakocinski, M, Marynowski, L et al. (1 more author) (2018) Mercury enrichments and the Frasnian-Famennian biotic crisis: A volcanic trigger proved? Geology, 46 (6). pp. 543-546. ISSN 0091-7613

https://doi.org/10.1130/G40233.1

Geology

Mercury enrichments and the Frasnian-Famennian biotic crisis: A volcanic trigger proved?

--Manuscript Draft--

Manuscript Number:	
Full Title:	Mercury enrichments and the Frasnian-Famennian biotic crisis: A volcanic trigger proved?
Short Title:	Frasnian-Famennian mercury anomalis and volcanism
Article Type:	Article
Keywords:	Frasnian-Famennian mass extinction; geochemistry; mercury anomalies; volcanism
Corresponding Author:	Grzegorz Racki, Ph.D. Uniwersytet Slaski w Katowicach Sosnowiec, Silesia POLAND
Corresponding Author Secondary Information:	
Corresponding Author's Institution:	Uniwersytet Slaski w Katowicach
Corresponding Author's Secondary Institution:	
First Author:	Grzegorz Racki, Ph.D.
First Author Secondary Information:	
Order of Authors:	Grzegorz Racki, Ph.D.
	Michał Rakociński
	Leszek Marynowski
	Paul Wignall
Order of Authors Secondary Information:	
Manuscript Region of Origin:	POLAND
Abstract:	The Frasnian-Famennian (F-F) global event, one of the five largest biotic crises of the Phanerozoic, has been inconclusively linked to rapid climatic perturbations promoted in turn by volcanic cataclysm, especially in the Viluy large igneous province (LIP) of Siberia. Conversely, trigger of four other Phanerozoic mass extinction intervals have decisively been linked to LIPs, owing to documented mercury anomalies, shown as the diagnostic proxy. Here we report multiple Hg enrichments in the two-step Late Frasnian (Kellwasser; KW) Crisis interval from paleogeographically distant successions in Morocco, Germany and northern Russia. The distinguishing signal, greater than 1 ppm in the domain of closing Rheic Ocean, is identified in different lithologies immediately below the F-F boundary, and approximately correlated with the onset of main extinction pulse. This key Hg anomaly, comparable only with an extreme spike known from the end-Ordovician extinction, is not controlled by increased bioproductivity in anoxic setting. We suggest, therefore, that global chemostratigraphic pattern near the F-F boundary records a greatly increased worldwide Hg input, controlled by Center Hill eruptive pulse of the Eovariscan volcanic acme, but likely not manifested exclusively by LIP(s). Consequently, all five major biotic crises of the Phanerozoic have now been more reliably linked to volcanic cataclysms.
Suggested Reviewers:	

Mercury enrichments and the Frasnian-Famennian biotic crisis: A volcanic trigger proved?

Grzegorz Racki[1*], Michał Rakociński[1], Leszek Marynowski[1], and Paul B. Wignall[2]
[1]Faculty of Earth Sciences, University of Silesia, ul. Będzińska 60, 41-200 Sosnowiec, Poland
[2]School of Earth Sciences, University of Leeds, Woodhouse Lane, Leeds LS2 9JT, United Kingdom

ABSTRACT

The Frasnian-Famennian (F-F) global event, one of the five largest biotic crises of the Phanerozoic, has been inconclusively linked to rapid climatic perturbations promoted in turn by volcanic cataclysm, especially in the Viluy large igneous province (LIP) of Siberia. Conversely, trigger of four other Phanerozoic mass extinction intervals have decisively been linked to LIPs, owing to documented mercury anomalies, shown as the diagnostic proxy. Here we report multiple Hg enrichments in the two-step Late Frasnian (Kellwasser; KW) Crisis interval from paleogeographically distant successions in Morocco, Germany and northern Russia. The distinguishing signal, greater than 1 ppm in the domain of closing Rheic Ocean, is identified in different lithologies immediately below the F-F boundary, and approximately correlated with the onset of main extinction pulse. This key Hg anomaly, comparable only with an extreme spike known from the end-Ordovician extinction, is not controlled by increased bioproductivity in anoxic setting. We suggest, therefore, that global chemostratigraphic pattern near the F-F boundary records a greatly increased worldwide Hg input, controlled by Center Hill eruptive pulse of the Eovariscan volcanic acme, but likely not manifested exclusively by LIP(s). Consequently, all five major biotic crises of the Phanerozoic have now been more reliably linked to volcanic cataclysms.

INTRODUCTION

The Frasnian-Famennian (F-F) stage boundary, traditionally linked with one of the five Phanerozoic mass extinctions, is often considered the final event of a long-term, stepwise collapse of Devonian metazoan reef ecosystems [Kellwasser (KW) Crisis, Fig. 1A; Hallam and Wignall, 1997; Gereke and Schindler, 2012; see the GSA Data Repository xxxxxxxxx, DR 1]. Recently, its status as a far more specific "biodiversity crisis," as determined by a drop in the speciation rate (see review in McGhee, 2013), has been emphasized. Current estimates of the magnitude of biodiversity losses by Stanley (2016), suggest that only ~ 40% of species vanished in the crisis. The prime causation of this global event remains conjectural, yet such kill factors as widespread transgressive anoxia and greenhouse climate interruption by two cooling pulses are widely accepted as part of an Earth-bound multi-causal scenario (Hallam and Wignall, 1997; Joachimski and Buggisch, 2002; Racki, 2005; McGhee, 2013; Ma et al., 2016; Song et al., 2017).

In terms of causation, the F-F turning point is often attributed lastly to volcanism possibly coupled with the effects of Eovariscan tectonism (Racki, 1998, 2005; Over, 2002; Pujol et al., 2006; Kravchinsky, 2012; Ricci et al., 2013; Winter, 2015; Ma et al., 2016). However, geological evidences, and especially geochemical proxies, on a global scale are unclear, and McGhee (2013, p. 148) summarized that "both the magnitude and timing of that volcanism remain at present unproved".

Refined insights into mercury chemostratigraphy over the past few years have resulted in its establishment as reliable indicator of the association of volcanic paroxysms and mass extinctions (Bergquist, 2017; for actualistic background see Pyle and Mather, 2003). Thus, volcanism as a major control for evolutionary turning points has emerged as a valid theory (Courtillot, 1999; Ernst, 2014; Wignall, 2015; Bond and Grasby, 2017). Only the F-F global event has remained an indecisive "missing link" in this respect. Here we report for the first time multiple Hg spikes from three sections that record the KW Crisis (Figs. 1B and 2), and focus on enrichments in the Upper KW (UKW) Level, directly below the crucial F-F boundary associated with major extinction step (Fig. 1A).

STUDY LOCALITIES AND METHODS

We have examined three sections, representing deep-water F-F successions (Fig. 1B; DR 2) that are marked by, at most, subordinate hiatuses: (1) Lahmida in Morocco, (2) Kahlleite in Germany, and (3) Siv'yu in north-eastern European Russia. The sections include different stratigraphic intervals. In contrast to the lower Frasnian - middle Famennian succession at Lahmida, the other sites only record the upper part of the KW interval. Therefore, this study focuses on the UKW mercury record, encompassing the upper part of the linguiformis conodont zone (Fig. 1A), with thicknesses between ~ 0.9 - 1 m (Kahlleite, Siv'yu) and ~2 m (Lahmida). A total of 121 samples were measured for Hg abundances at the Faculty of Earth Sciences, University of Silesia (Poland), using atomic absorption spectrometry (AAS) analyzer Milestone DMA-80 Direct Mercury (detection limit = 0.2 ppb; for more detail of all methods see DR 3).

Mercury has a high affinity to organic matter, and to a lesser extent with sulfides and clay minerals (Bergquist, 2017). Thus, Hg enrichment is best depicted by normalizing to total organic carbon (TOC) (Sanei et al., 2012; Sial et al., 2016; Percival et al., 2017). An Eltra CS-500 IR-analyzer at the University of Silesia was used for TOC determination; in addition, Al and Mo contents were analyzed as well (DR 2 and 3). Our analytical data therefore allow testing for correlation between Hg values and TOC and clay minerals (Al). Comparison with Mo abundances (as an approximation of sulfide content) also allows for the potential effect of pyrite on Hg drawdown. Enrichment patterns are considered for samples revealing contents distinctly greater than background in the succession (= threefold median value as a granted threshold). The recurrence of enrichment factors (EFs) larger than 3 for Hg/TOC (emphasized herein; Fig. 2) and Hg/Al_2O_3 ratios, along with less rigorously considered high absolute Hg abundances, helps identify samples as truly Hg enriched one (DR 2).

RESULTS

The KW Crisis interval within the shale-limestone succession exposed at Lahmida, Morocco, displays multiple Hg spikes that also remain when normalized for TOC variation (Fig. 2A). Enriched Hg abundances can also be observed elsewhere in the section, including a peak value just below KW Frasnian deposits (1145 ppb), but these are largely not confirmed in Hg/TOC plots. At the Kahlleite section in Germany, Hg and Hg/TOC values are low except in a thin UKW black shale at the F-F boundary (this is a unique horizon in this limestone-dominated section) where a sharp spike is seen (2517 ppb; Fig. 2A-B).

The Uralian Syv'yu section, marked by lithological variation from black shale to grey limestones and chert, includes several far less Hg enriched horizons (up to 260 ppb Hg), notably in the upper, limestone half, of the UKW interval (Fig. 2C). The enrichments extend up to a few centimeters below the F-F boundary are relatively minor (121 ppb), but distinctly recorded in Hg/TOC ratios (EF= 4.2). Conversely, organic- and clay-rich portion of lower part of UKW is relatively Hg impoverished.

POSSIBLE CAUSAL LINK TO VOLCANISM: DISCUSSION

Previously volcanism as a contributor to the F-F biotic crisis has not been considered important (Walliser, 1996; Hallam and Wignall, 1997; Courtillot, 1999; Averbuch et al., 2005; Becker et al., 2012; McGhee, 2013). This view reflects not only the imprecise datings of volcanic events around the F-F stage boundary, but also the suppressed volcanic signatures in reliably dated sites (in contrast to the pyroclastic-rich Devonian-Carboniferous boundary beds for example; Marynowski et al., 2012). However, rifting episodes and associated volcanic activity has been recorded in several regions (Johnson, 1988; Racki 1998, 2005; Over, 2002; Pujol et al., 2006), and more recently dating of the F-F boundary (376.1 ± 3.6 Ma, Kaufmann, 2006; 372.2 ± 1.6 Ma; Becker et al., 2012) and Devonian LIPs (Fig. 1B) and other types of magmatic activity (including kimberlites) has shown a close temporal coincidence. In particular, Ricci et al. (2013) established an age of paroxysmal emplacement of the key Viluy (or Yakutsk) LIP as 376.7 ± 1.7 Ma. Furthermore, Winter (2015) reported numerous thin metabentonites in Central European successions, including the Center Hill (CH) eruptive episode just prior to the F-F boundary (Over, 2002; Fig.1A), that appear to record intensified alkaline volcanism during the KW interval.

Therefore, there a several candidates for an F-F volcanic “smoking gun” although geochronological dating needs considerable improvement. Geochemical proxies documented hitherto from several F-F sections, including Zr/Al and Sr isotopes (Racki et al., 2002; Chen et al., 2005; Pujol et al., 2006; Weiner et al., 2017), and mineralogical data (Yudina et al., 2002), are additional but far from conclusive evidence. Thus, the emergence of Hg chemostratigraphy as a reliable proxy for the occurrence of major volcanic events during mass extinction episodes. Moreno et al. (2018) have reported enriched interval (up to 1570 ppb Hg) around the UKW level from coastal facies of Catalan Spain, which they interpreted as a signature of hydrothermal activity.

Our results reveal multiple anomalous Hg abundances in excess of 1 ppm in the stratigraphic interval corresponding to the major extinction pulse of KW Crisis in two distant regions (Morocco, Germany). Moreover, another site from remote northern Laurussian domain (Subpolar Urals) also records second-order Hg excursions in UKW level. These Hg anomalies are 3 to 7.5 times the background (= median value) in particular sections (but peak at 122 in Kahlleite), and are similarly seen in Hg/TOC ratios (EF=15 in Lahmida). Importantly, this prominent signal is associated with different lithologies showing contrasting values of main Hg control proxies, ranging from black shale at Kahlleite (Al_2O_3 = 17.2 %, TOC = 7%; Mo = 41 ppm) to organic-poor marly limestone at Lahmida (2.3, 0.2, 5, respectively) to pure UKW limestones at Syv'yu (for the top value: 0.4, 2.3, <5, respectively). Therefore, although interregional variability is considerable, the Hg spikes occur in diverse F-F lithologies that contrast with the Hg-impoverished 'quiet' Famennian stage. In our studied sites, background levels vary from 20.7 ppb (Kahlleite) to 153.2 ppb (Lahmida). Notably, Wedepohl's (1991) averaged Phanerozoic Hg concentrations range from 30 ppb (limestone) to 450 ppb (argillaceous shale).

In summary, Hg abundances in our study sections do not correlate with organic matter and/or anoxic conditions, nor with clay content (r less than 0.5; DR 2). Only at Syv'yu is their a possible link of Hg enrichment with a Zr-bearing, 0.5 m thick interval of possible partly volcaniclastic origin (Yudina et al., 2002). Thus, in accord with the interpretation of Hg spikes associated with other biotic crises (Nascimento-Silva et al., 2011; Sanei et al., 2012; Grasby et al., 2015; Sial et al., 2016; Percival et al., 2017; Bergquist, 2017), the Hg and/or Hg/TOC signals found immediately below the F-F boundary are attributed to a major volcanic pulse, such as a LIP, and tentatively correlated with the CH eruptive episode (Fig. 2). Multiple Hg-enriched horizons (as many as five at the Uralian succession) imply pulsed volcanic paroxysms, although this detail may be obscured in the condensed European sections. Thus, indicates a duration of F-F volcanism of around 100 Ka (using the chronological scheme of De Vleeschouwer et al., 2017). Older Frasnian eruptive events, recognized by Winter (2015), can also be tentatively identified, in particular pre-KW (Pictor) eruption at Lahmida (Fig. 2A). A similar connection has recently been made for the end-Ordovician crisis, even though conclusive evidence of a coeval LIP is lacking at this time (Jones et al., 2017).

The studied F-F Hg signatures are associated with unstable, super-greenhouse conditions (Joachimski and Buggisch, 2002; Chen et al., 2005; Racki, 2005; McGhee, 2013; Ma et al., 2016; Song et al., 2017). These climate oscillations may have been driven by diverse volcanism- and tectonics-driven feedbacks, such as fertilization of the ocean surface water (Courtillot, 1999;

Over, 2002; Averbuch et al., 2005; Winter, 2015). A volcanism-promoted cooling scenario, with obvious implications for the F-F global event, was discussed recently for the end-Ordovician extinction by Jones et al. (2017). In their interpretation, the trigger phase of eruptive volcanism is said to precede the inception of cooling and biodiversity collapse (via weathering and ice albedo feedbacks). This scenario may be manifest in the F-F section studied at Lahmida.

CONCLUSIONS

Our study provides the first worldwide evidence of a major phase of volcanogenic Hg injection into the atmosphere during the F-F mass extinction boundary, thus lending support to the postulated relationship of LIP volcanism and global crises for all of the “Big Five” crises. The greatest Hg concentrations, potentially associated with the Center Hill volcanic event in the domain of closing Rheic Ocean (Winter, 2015; Raumer et al., 2017; Fig. 1B), are comparable to the extreme Hg and Hg/TOC values reported from the end-Ordovician extinction (DR 4). The contemporaneous, multiple-phase magmatic emplacement during the acme of Eovariscan volcano-tectonic activity (Racki, 1998, 2005; Averbuch et al., 2005), may indicate that volcanic source of Hg enrichment was not attributable entirely or solely to the Viluy LIP. The complicated temporal pattern of the potential volcanic signatures, encompassing both explosive and effusive activity, provides a rationale for further high-resolution study in particular regions and through the whole KW Crisis, but a such attempt will be certainly challenged by condensed/discontinuous nature of the F-F passage (recording the worldwide carbonate crisis; Racki et al., 2002). Future research should focus on multiproxy tests to determine a possible volcanogenic source for the recognized Hg signals, using Hg and Sr isotope systematics, among others.

ACKNOWLEDGMENTS

The study was supported by the MAESTRO grant 2013/08/A/ST10/00717 from the National Science Centre – Poland (to Grzegorz Racki). We warmly thanks Zdzisław Bełka, Manfred Gereke, and other participants in the grant field works. Alexandra Yudina kindly provided samples from the Uralian section. Insightful comments from Lawrence Percival, Karl Főllmi, Zdzisław Bełka, as well as Vincent Courtillot and three anonymous journal reviewers improved the manuscript.

REFERENCES CITED

Averbuch, O., Tribovillard. N., Devleeschouwer. X., Riquier, L., Mistiaen, B., and van Vliet-Lanoe, B., 2005, Mountain building-enhanced continental weathering and organic carbon burial as major causes for climatic cooling at the Frasnian–Famennian boundary (ca 376 Ma BP): Terra Nova, v. 17, p. 25–34, doi: 10.1111/j.1365-3121.2004.00580.x.

Becker, R.T., Gradstein, F.M., and Hammer, O., 2012, The Devonian Period, in Gradstein, F.M., et al., eds., The Geologic Time Scale 2012: Amsterdam, Elsevier, v. 2, p. 559–601, doi: 10 .1016 /B978 -0 -444 -59425 -9 .00022 -6.

Bergquist, A.B., 2017, Mercury, volcanism, and mass extinctions: Proceedings of the National Academy of Sciences of the United States of America, v. 114 (33), p. 8675-8677, doi: 10.1073/pnas.1709070114 114 no. 33.

Bond, D.P.G. and Grasby, S.E., 2017, On the causes of mass extinctions: Palaeogeography, Palaeoclimatology, Palaeoecology, v. 478, p. 3-29, doi: 10.1016/j.palaeo.2016.11.005.

Chen, D., Qing, H., and Li, R., 2005, The Late Devonian Frasnian–Famennian (F/F) biotic crisis: insights from δ^{13} C_{carb}, δ^{13} C_{org} and ^{87} Sr/^{86} Sr isotopic systems: Earth and Planetary Science Letters, v. 235, p. 151-166, doi:10.1016/j.epsl.2005.03.018.

Courtillot, V., 1999, Evolutionary Catastrophes: The Science of Mass Extinctions: Cambridge, Cambridge University Press, 173 p., doi: 10.1029/2003EO210009.

De Vleeschouwer, D., da Silva, A.C., Sinnesael, M., Chen, D., Day, J.E., Whalen, M.T., Guo, Z., and Claeys, P., 2017, Timing and pacing of the Late Devonian mass extinction event regulated by eccentricity and obliquity: Nature Communications, v. 8, p. 1-11, doi: 10.1038/s41467-017-02407-1.

Dopieralska, J., 2003, Neodymium isotopic composition of conodonts as a palaeoceanographic proxy in the Variscan oceanic system: Ph.D. Thesis, Justus-Liebig-University, Giessen, 111 p.

Ernst, R.E., 2014, Large Igneous Provinces: Cambridge, Cambridge University Press, 653 p, doi: 10.1017/CBO9781139025300.

Gereke, M., 2004, Das Profil Kahlleite Ost - die stratigraphische Entwicklung einer Tiefschwelle im Oberdevon des Bergaer Sattels (Thüringen): Geologica et Palaeontologica, v. 38, p. 1–31.

Gereke, M., and Schindler, E., 2012, "Time-Specific Facies" and biological crises — The Kellwasser Event interval near the Frasnian/Famennian boundary (Late Devonian): Palaeogeography, Palaeoclimatology, Palaeoecology, v. 367–368, p. 19–29, doi: 10.1016/j.palaeo.2011.11.024.

Golonka, J., Ross, M.I., and Scotese, C.R., 1994, Phanerozoic paleogeographic and paleoclimatic modeling maps, in Embry, A.F., Beauchamp, B. and Glass, D.J., eds., Pangea: Global environment and resources Canadian Society of Petroleum Geologists Memoir 17, p. 1–47.

Grasby, S.E., Beauchamp, B., Bond, D.P.G., Wignall, P.B., and Sanei, H., 2015, Mercury anomalies associated with three extinction events (Capitanian crisis, latest Permian extinction and the Smithian/Spathian extinction) in NW Pangea: Geological Magazine, v. 153, p. 285–297, doi: 10 .1017 /S0016756815000436.

Hallam, A., and Wignall, P.B., 1997, Mass Extinctions and Their Aftermath: Oxford, Oxford University Press, 328 p.

Joachimski, M.M., and Buggisch, W., 2002, Conodont apatite δ^{18}O signatures indicate climatic cooling as a trigger of the Late Devonian mass extinction: Geology, v. 30, p. 711–714, doi: 10.1130/0091-7613(2002)030<0711:CAOSIC>2.0.CO;2.

Johnson, J.G., 1988, Letters: Volcanism, eustacy, and extinctions: Geology, v. 16, p. 573–574, doi: 10.1130/0091-7613(1988)016<0572:L>2.3.CO;2.

Jones, D.S., Martini, A.M., Fike, D.A., and Kaiho, K., 2017, A volcanic trigger for the Late Ordovician mass extinction? Mercury data from south China and Laurentia: Geology, v. 45, p. 631-634, doi:10.1130/G38940.1.

Kaufmann, B., 2006, Calibrating the Devonian Time Scale: A synthesis of U-Pb ID-TIMS ages and conodont stratigraphy: Earth-Science Reviews, v. 76, 175–190, doi: 10.1016/j.earscirev.2006.01.001

Kravchinsky, V.A., 2012, Paleozoic large igneous provinces of Northern Eurasia: Correlation with mass extinction events: Global and Planetary Change, v. 86-87, p. 31–36, doi:10.1016/j.gloplacha.2012.01.007.

Ma, X., Gong, Y., Chen, D., Racki, G., Chen, X., and Liao, W., 2016, The Late Devonian Frasnian-Famennian Event in South China—Patterns and causes of extinctions, sea level changes, and isotope variations: Palaeogeography, Palaeoclimatology, Palaeoecology, v. 448, p. 224–244, doi: 10 .1016 /j .palaeo .2015 .10 .047.

Marynowski, L., Zatoń, M., Rakociński, M., Filipiak,P., Kurkiewicz, S., and Pearce, T.J., 2012, Deciphering the upper Famennian Hangenberg Black Shale depositional environments based on multi-proxy record: Palaeogeography, Palaeoclimatology, Palaeoecology, v. 346–347, p. 66–86, doi: 10.1016/j.palaeo.2012.05.020 .

McGhee, G.R., 2013, When the Invasion of Land Failed: The Legacy of the Devonian Extinctions: New York, Columbia University Press, 336 p.

Moreno, C., Gonzalez, F., Sáez, R., Melgarejo, J.C., and Suárez-Ruiz, I., 2018.The Upper Devonian Kellwasser Event recorded in a regressive sequence from inner shelf to lagoonal pond, Catalan Coastal Ranges, Spain: Sedimentology, v. 65, in press, doi: 10.1111/sed.12457.

Nascimento-Silva, M.V., Sial, A.N., Ferreira, V.P., Neumann, V.H., Barbosa, J.A., Pimentel, M.M., and de Lacerda, L.D., 2011, Cretaceous-Paleogene transition at the Paraíba Basin, Northeastern, Brazil: Carbon-isotope and mercury subsurface stratigraphies: Journal of South American Earth Sciences, v. 32, p. 379–392, doi: 10.1016/j.jsames.2011.02.014.

Over, D.J., 2002. The Frasnian/Famennian boundary in central and eastern United States. Palaeogeography, Palaeoclimatology, Palaeoecology, v. 181, p. 153–169, doi: 10.1016/S0031-0182(01)00477-1.

Percival, L.M.E., Witt, M.L.I., Mather, T.A., Hermoso, M., Jenkyns, H.C., Hesselbo, S.P., Al-Suwaidi, A.H., Storm, M.S., Xu, W., and Ruhl, M., 2015, Globally enhanced mercury deposition during the end-Pliensbachian extinction and Toarcian OAE: A link to the Karoo–Ferrar Large Igneous Province: Earth and Planetary Science Letters, v. 428, p. 267–280, doi: 10 .1016 /j .epsl .2015 .06 .064

Percival, L.M.E., Ruhla, M., Hesselbo, S.P., Jenkyns, H.C., Mather, T.A., and Whiteside J.H., 2017, Mercury evidence for pulsed volcanism during the end-Triassic mass extinction: Proceedings of the National Academy of Sciences of the United States of America, v. 114, p. 7929–7934, doi: 10.1073/pnas.1705378114.

Pujol, F., Berner, Z., and Stüben, D., 2006, Palaeoenvironmental changes at the Frasnian/Famennian boundary in key European sections: chemostratigraphic constraints: Palaeogeography, Palaeoclimatology, Palaeoecology, v. 40, p. 120–145, doi:10.1016/j.palaeo.2006.03.055.

Pyle, D.M., and Mather, T.A., 2003, The importance of volcanic emissions for the global atmospheric mercury cycle: Atmospheric Environment, v. 37, p. 5115–5124, doi:10.1016/j.atmosenv. 2003.07.011.

Racki, G., 1998, Frasnian-Famennian biotic crisis: Undervalued tectonic control?: Palaeogeography, Palaeoclimatology, Palaeoecology, v. 141, p. 77–198, doi: 10.1016/S0031-0182(98)00059-5.

Racki, G., 2005, Toward understanding Late Devonian global events: Few answers, many questions, in Over. D.J., Morrow, J.R., and Wignall, P.B., eds., Understanding Late Devonian and Permian–Triassic Biotic and Climatic Events: Towards an Integrated Approach, Developments in Palaeontology and Stratigraphy 20, p. 5–36.

Racki, G., Racka, M., Matyja, H., and Devleeschouwer, X., 2002, The Frasnian/Famennian boundary interval in the South Polish–Moravian shelf basins: Integrated event-stratigraphical approach: Palaeogeography, Palaeoclimatology, Palaeoecology, v. 181, p. 251–297, doi: 10 .1016 /S0031 -0182 (01)00481 -3.

Raumer, J.F., Nesbor, H.D., and Stampfli, G.M., 2017, The north-subducting Rheic Ocean during the Devonian: Consequences for the Rhenohercynian ore sites: International Journal of Earth Sciences, v. 106, p. 2279–2296, doi:10.1007/s00531-016-1425-x

Ricci, J., Quidelleur, X., Pavlov, V., Orlov, S., Shatsillo, A., and Courtillot, V., 2013, New ^{40}Ar/^{39}Ar and K–Ar ages of the Viluy traps (Eastern Siberia): Further evidence for a relationship with the Frasnian–Famennian mass extinction: Palaeogeography, Palaeoclimatology, Palaeoecology, v. 386, p. 531–540, doi: 10.1016/j.palaeo.2013.06.020.

Sanei, H., Grasby, S.E., and Beauchamp, B., 2012, Latest Permian mercury anomalies: Geology, v. 40, p. 63–66, doi:10.1130/G32596.1.

Sial, A.N., Chen, J., Lacerda, L.D., Frei, R., Tewari, V.C., Pandit, M.K., Gaucher, C., Ferreira, V.P., Cirilli, S., Peralta, S., Korte, C., Barbosa, J.A., and Pereira, N.S., 2016, Mercury enrichment and Hg isotopes in Cretaceous–Paleogene boundary successions: Links to volcanism and palaeoenvironmental impacts: Cretaceous Research, v. 66, p. 60–81, doi: 10.1016/j.cretres.2016.05.006.

Song H.J., Algeo, T.J., Tong, J.N., Romaniello, S.J., Zhu, Y.Y., Chu, D.L., and Anbar, A.D., 2017, Uranium and carbon isotopes document global-ocean redox-productivity relationships linked to cooling during the Frasnian-Famennian mass extinction. Geology, v. 45, p. 887-890, doi: 10.1130/G39393.1.

Stanley, S.M., 2016, Estimates of the magnitudes of major marine mass extinctions in earth history: Proceedings of the National Academy of Sciences of the United States of America, v. 113, p. 6325–6334, doi: 10.1073/pnas.1613094113.

Walliser, O.H., 1996, Global events in the Devonian and Carboniferous, in Walliser, O.H., ed., Global Events and Event Stratigraphy in the Phanerozoic: Springer, Berlin-Heidelberg-New York, p. 225-250.

Wedepohl, K.H., 1991, The composition of the upper earth's crust and the natural cycles of selected metals. Metals in natural raw materials. Natural resources, in Merian, E., ed., Metals and their Compounds in the Environment: Verlag Chemie (VCH), Weinheim, p. 3–17.

Weiner, T., Kalvoda, J., Kumpan, T., Schindler, E., and Šimíček, D., 2017, An integrated stratigraphy of the Frasnian-Famennian boundary interval (Late Devonian) in the Moravian Karst (Czech Republic) and Kellerwald (Germany): Bulletin of Geosciences, v. 92, p. 257–281, doi: 10.3140/bull.geosci.1636.

Wignall, P.B., 2015, The Worst of Times: How Life on Earth Survived 80 Million Years of Extinctions: Princeton, Princeton University Press, 199 p.

Winter, J., 2015, Vulkanismus und Kellwasser-Krise – Zirkon-Tephrostratigrafie, Identifizierung und Herkunft distaler Fallout-Aschenlagen (Oberdevon, Synklinorium von Dinant, Rheinisches Schiefergebirge, Harz): Zeitschrift der Deutschen Gesellschaft für Geowissenschaften, v. 166, p. 227–251, doi: 10.1127/1860-1804/2015/0092.

Yudina, A.B., Racki, G., Savage, N.S., Racka, M., and Małkowski, K., 2002, The Frasnian-Famennian events in a deep-shelf succession, Subpolar Urals: Biotic, depositional and geochemical records: Acta Palaeontologica Polonica, v. 47, p. 355–372.

FIGURE CAPTIONS:

Fig. 1. A. Scheme of the F–F global event and the two-step Kellwasser Crisis (based on Gereke and Schindler, 2012; DR 1), and related volcanic events after Winter (2015, fig. 2). B. Locations of the F-F sites studied for Hg abundances, compared to inferred proximity to coeval large igneous provinces (LIPs; after Kravchinsky, 2012, and Ernst, 2014; Late Devonian paleogeography after Golonka et al., 1994).

Fig. 2. Reference F-F sections in Morocco (A; after Dopieralska, 2003), Germany (B; after Gereke, 2004) and Russia (C; after Yudina et al., 2002) showing Hg enrichments associated with the KW Crisis interval (DR 2), with emphasis on likely volcanic Center Hill (CH) signal near the F-F boundary (volcanic events after Winter, 2015; Sc – Scorpius, Sx – Sextans; PPP – Pictor-Phoenix-Pegasus; Fig. 1A).

Figure 1

Click here to download Figure Racki et al Figure 1 FINAL.tif

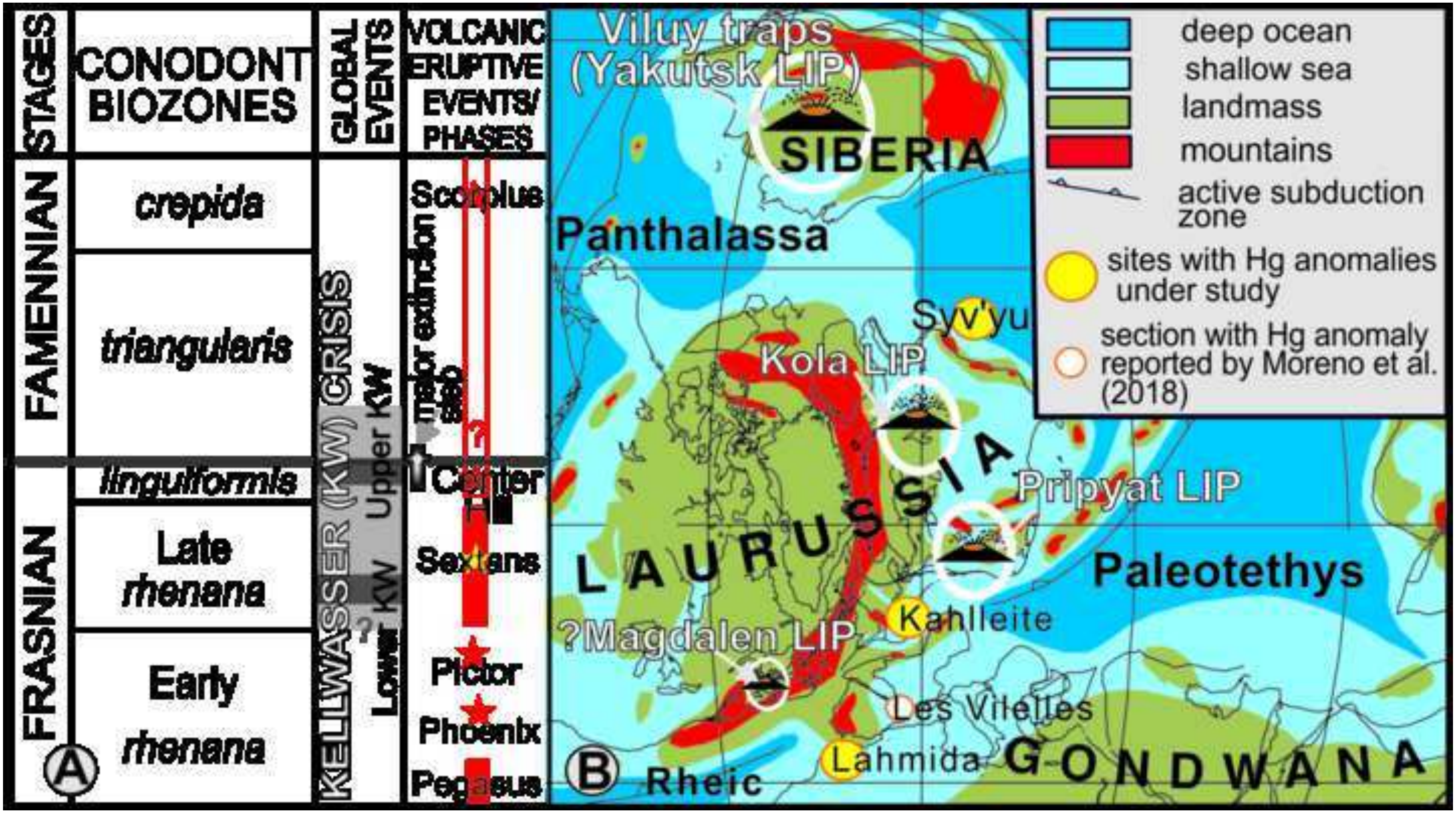

Figure 2

Click here to download Figure Racki et al. Figure 2 FINAL.tif

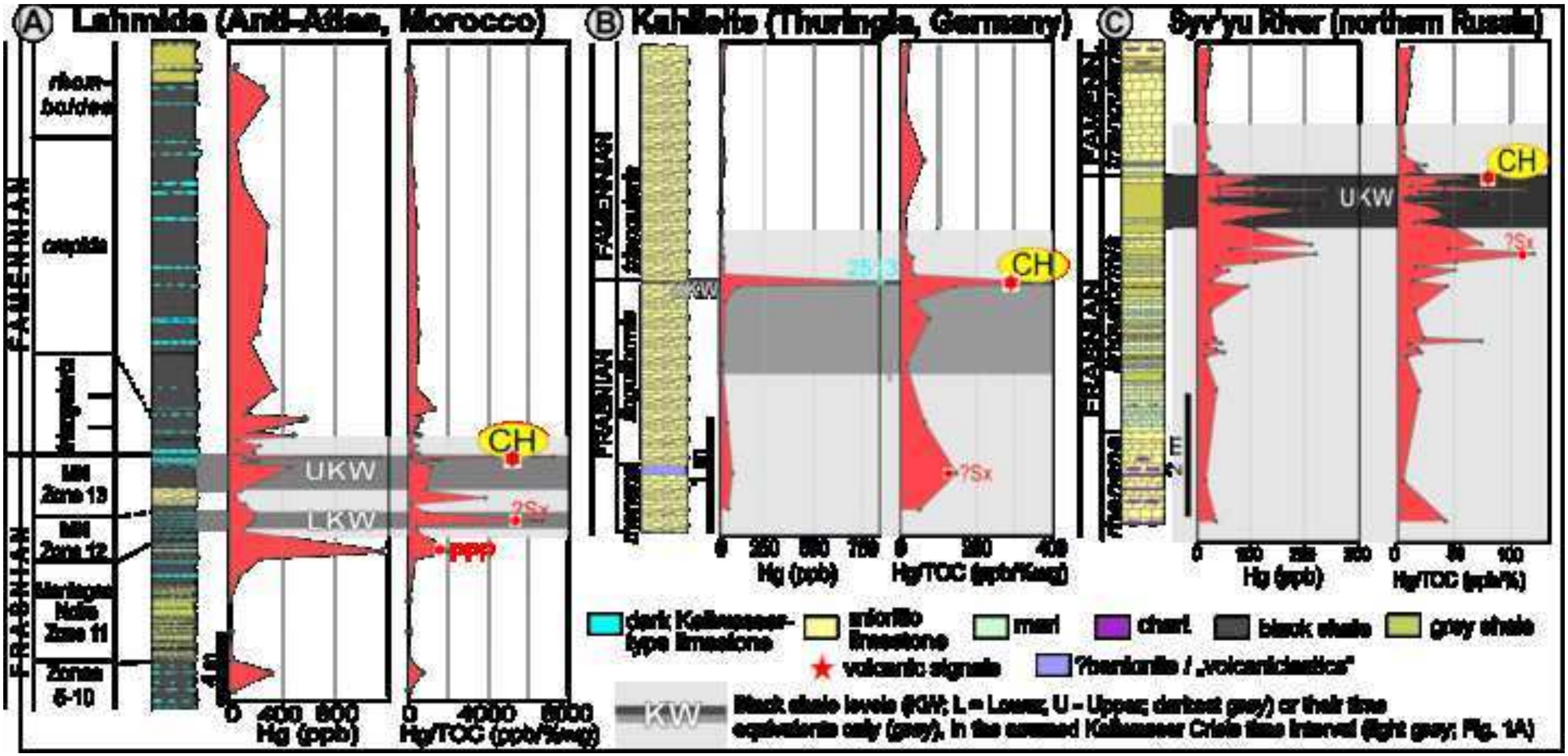

SUPPLEMENTARY DATA

Mercury enrichments and the Frasnian-Famennian biotic crisis: A volcanic trigger proved?

Grzegorz Racki, Michał Rakociński, Leszek Marynowski. Paul B. Wignall

(DR 1) SCHEME OF THE FRASNIAN-FAMENNIAN GLOBAL EVENT

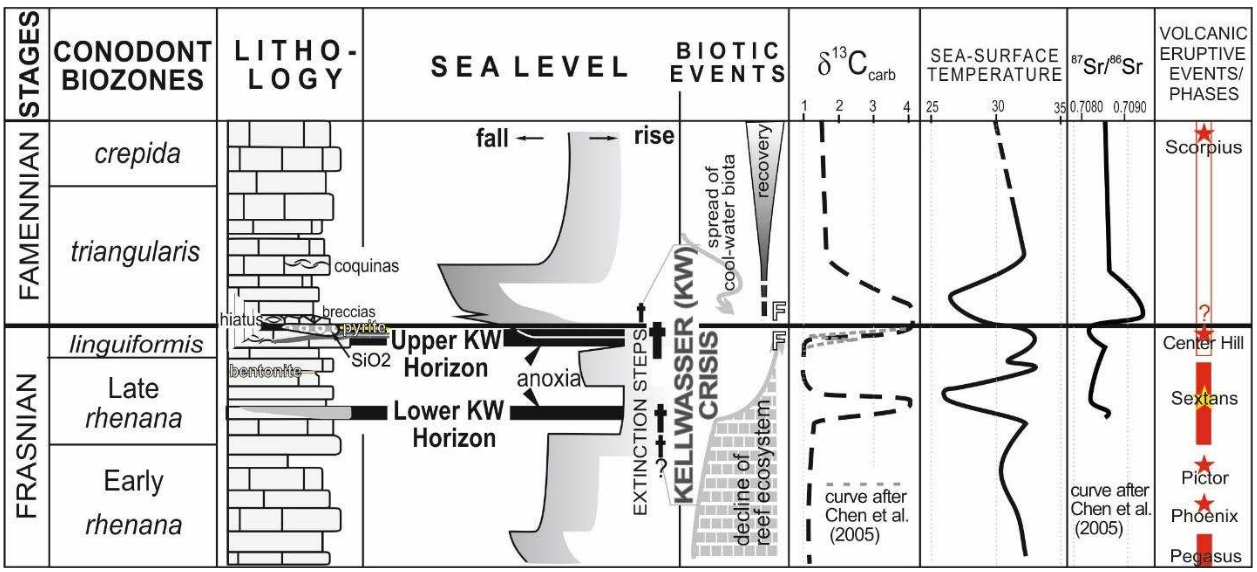

Diagram showing composite sedimentary and geochemical records across the Frasnian–Famennian transition, and major eustatic and biotic events (modified fig. 3 from Racki, 2005, and references therein; compare Joachimski and Buggisch, 2002, fig. 2; Gereke and Schindler, 2012, fig. 1 and 9; Ma et al., 2016, fig. 11); volcanic events after Winter (2015, fig. 2).

(DR 2) ANALYTICAL SECTIONS

The successions listed below were recently studied, in different extent, within the program of MAESTRO grant 2013/08/A/ST10/00717 (to Grzegorz Racki) from Polish National

Science Foundation. Archival samples only from German and Russian localities were re-analyzed recently for Hg abundances.

Enrichment Hg patterns are shown for samples revealing values distinctly greater than background (= threefold median value as a given threshold; cf. Riboulleau et al., 2018) in the succession. The recurrence of enrichment factors larger than 3 for Hg/TOC and Hg/Al_2O_3, along with less rigorously determined values for absolute Hg abundances, identifies the highlighted sample in tables below as truly enriched one (or likely/possibly enriched one, where not all requirements are fulfilled). On the other hand, the distinctive Hg impoverishment in at least one of these test indicators eliminates the sample from consideration as enriched.

The statistical calculations were carried out using PAST 1.94b (Hammer, 2009); significant correlations with a p-value less than 0.01 are given in bold type.

In the tables below, time intervals of the anoxic Kellwasser events are highlighted in light grey, whilst black shale facies is shown in dark grey.

1. Lahmida section, eastern Anti-Atlas, Morocco

Coordinates: 31°30'67.0'' N; 4°19'26.2'' W

The Lahmida section, located ca. 12 km to north-west from Erfoud in the eastern part of the Anti-Atlas, accumulated on the deep-water Rheiris shelf basin, which stretched to north from Tafilalt Platform (Dopieralska, 2003, 2009). The investigated succession stratigraphically extends from the lower Frasnian - MN Zone 4 to the middle Famennian rhomboidea Zone (see Dopieralska, 2003). The succession consists mainly of monotonous shales with numerous marly interbeds and concretion horizons as well as dark gray limestones, which together with dark gray shales represent the Kellwasser facies of the Rheris Basin (Wendt and Belka, 1991; for more details about geology see Dopieralska, 2003). We analyzed 43 samples, collected in 2014 and 2015 for the MAESTRO grant with the help of Zdzisław Bełka.

Hg, TOC, Al_2O_3, Mo contents, Hg/TOC, Hg/Al_2O_3 ratios, and $\delta^{13}C$ data from F-F succession at Lahmida.

Stage	Sample	Hg	TOC	Al_2O_3	Mo			
	Method	AAS	Eltra CS-	ICP-ES	ICP-MS			
		ppb	%	%	ppm			

	Max. detection limit (MDL)	0.2	0.01	0.01	0.1	**Hg/TOC**	**Hg/ Al_2O_3**	**Height (cm)**
	LA 44	54.5	0.61	4.83	1.0	89.3	11.3	3575
	LA 43/44	31.2	0.68	5.23	1.3	45.9	6.0	3555
	LA 42	250.0	0.83	5.85	4.4	301.2	42.7	3455
	LA 41/42	276.6	1.14	21.90	5.8	242.6	12.6	3405
	LA 40T	44.8	0.59	3.37	0.3	75.9	13.3	3159
	LA 38	99.8	0.42	2.93	0.9	237.6	34.1	2918
	LA 35/36B	283.2	0.83	20.60	0.7	341.2	13.7	2687
	LA 34	260.0	0.75	5.50	0.3	346.7	47.3	2350
	LA 32/33	207.0	0.46	20.72	1.4	450.0	10.0	2093
	LA 32M	153.2	0.38	2.61	1.5	403.2	58.7	2040
	LA 30	333.8	0.86	3.58	1.6	388.1	93.2	1781
	LH 29	137.5	0.11	1.73	4.6	1250.0	79.5	1670
	LH 28	114.0	0.40	5.41	1.1	285.0	21.1	1635
	LH 27A2	569.1	0.93	21.04	1.9	611.9	27.0	1614
	LA 27/28	338.4	1.05	20.70	2.7	322.3	16.3	1569
	LH 27	126.4	0.77	4.97	4.9	164.2	25.4	1538
	LA 26/27	481.2	0.86	21.02	2.3	559.5	22.9	1516
	LH 26	57.3	0.55	2.43	3.3	104.2	23.6	1497
	LA 25/26	232.5	0.54	18.85	2.5	430.6	12.3	1464
	LH 25T	180.1	0.79	3.10	0.9	228.0	58.1	1437
FAMENNIAN	LH 25B	189.3	0.37	2.57	2.3	511.6	73.7	1423
FRASNIAN	LA 24/25S	36.9	0.35	3.17	1.6	105.4	11.6	1413
	LA 24/25N **CH**	1136.4	0.16	2.33	0.9	7102.5	487.7	1403
	LH 24T	113.2	0.65	2.79	2.0	174.2	40.6	1395
	LH 24B **?**	153.7	0.10	0.96	0.9	1537.0	160.1	1383
Upper KW	LH 23T	219.0	0.67	1.99	4.4	326.9	110.1	1374
	LH 23B	90.0	0.13	4.24	9.9	692.3	21.2	1366
	LH 22 **?**	464.2	0.41	2.08	15.0	1132.2	223.2	1343
	LH 21	90.3	0.11	3.21	3.1	820.9	28.1	1215
	LH 20	45.7	0.01	2.41	1.2	4570.0	19.0	1178
	LH 19	123.0	0.76	2.49	1.3	161.8	49.4	1138
	LH 18	187.7	0.20	0.93	5.0	938.5	201.8	1089
	LA 17/18T**?Sx**	183.2	0.03	1.04	1.6	6106.7	176.2	1045
Lower KW	LA 17/18B	147.8	0.37	1.61	1.5	399.5		1020
	LA 17M	99.9	0.24	2.75	2.0	416.3	36.3	989
	LA 14 **PPP**	1144.9	0.56	3.49	4.6	2044.5	328.1	875
	LA 13T	233.1	0.71	1.05	1.7	328.3	222.0	836
	LA 12	68.8	0.41	3.78	0.5	167.8	18.2	735
	LA 10	6.8	0.32	2.09	0.5	21.3	3.3	602
	LA 8	9.9	0.28	1.71	<0.1*	35.4	5.8	418
	LA 6	25.9	0.33	2.29	0.2	78.5	11.3	268
	LA 5	312.3	0.48	1.55	3.1	650.6	201.5	198
	LA 4A	36.9	1.21	1.84	1.6	30.5	20.1	101
Median value		**153.2**	0.48	2.93	1.6	341.2	28.1	
Spearman's rs correlation coefficient coefficient		Hg	0.37	0.24	**0.40**			

*Mo assumed as 0.09 ppm for purpose of the correlation calculation

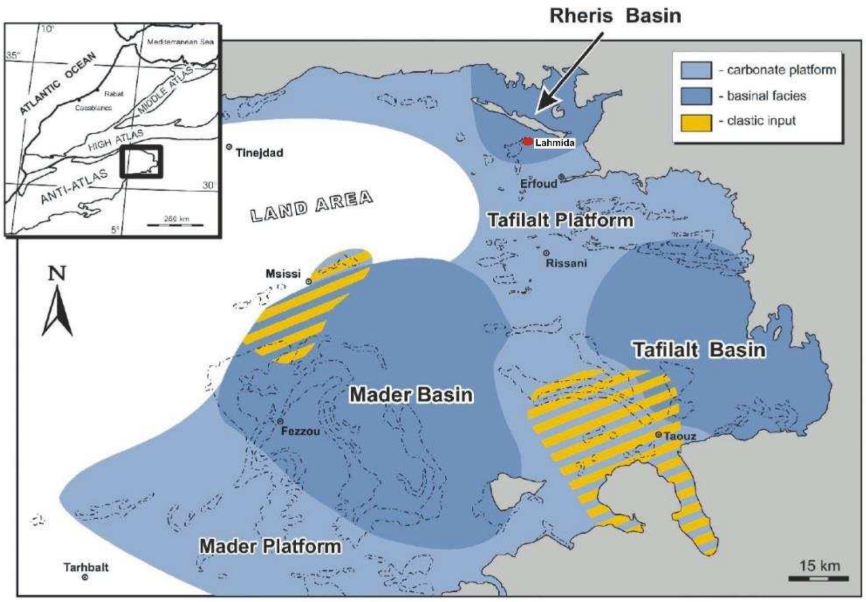

S 1. Geographic and palaeogeographic location of the Lahmida section (Bełka and Wendt, 1992; Dopieralska, 2003).

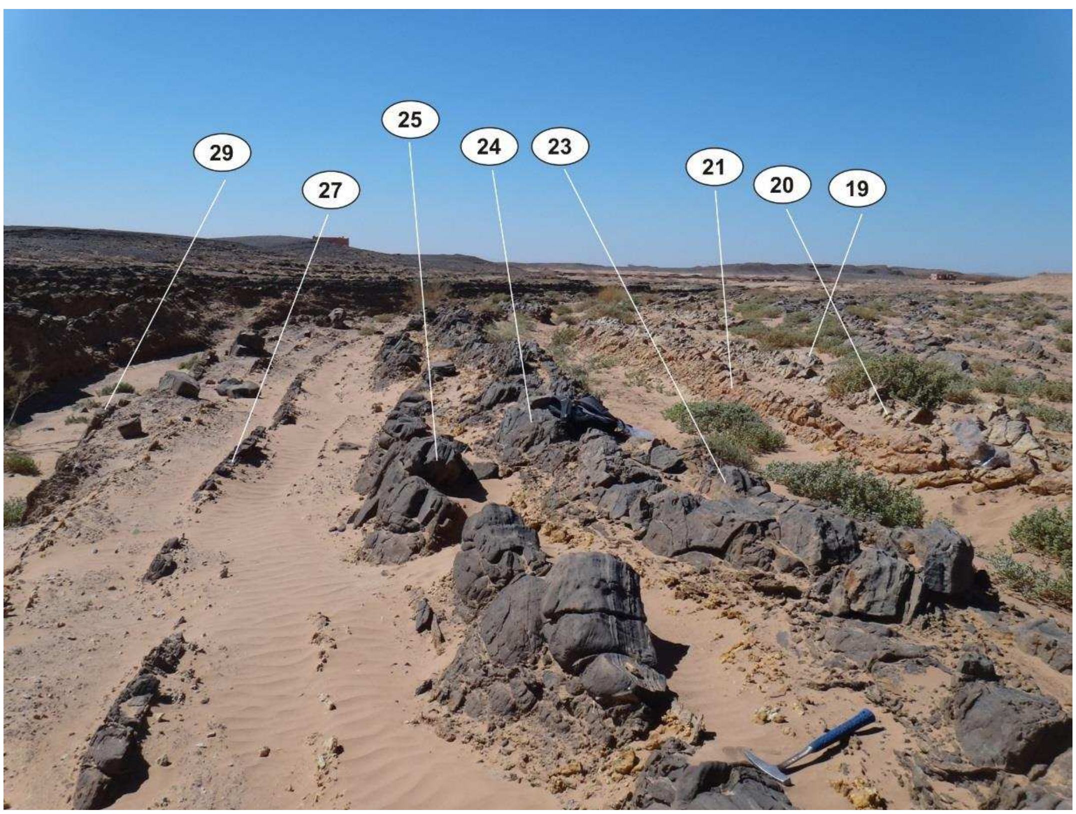

S 2. The Frasnian-Famennian boundary beds at Lahmida section (March 2014), with the stage boundary located between beds 24 and 25. Photo courtesy Z. Bełka.

2. Kahlleite, Thuringia, Germany

Coordinates: 50°37’32.5’’; N; 11°50’32.2’’ E

The Frasnian-Famennian transition at inactive (since 2013) Kahlleite quarry, 1 km to south-west from Rüdersdorf near Gera, Thuringia, was studied in detail by Gereke (2004, 2007). The mainly limestone strata of the north-west flank of Berga Anticline deposited on a deep submarine rise (Gereke and Schindler, 2012). This locality was sampled in 2012 by L.M. and M.R., guided by Manfred Gereke, and 17 samples were recently re-studied for Hg.

Hg, Al_2O_3, Mo contents, and Hg/TOC and Hg/Al_2O_3 ratios from F-F succession at Kahlleite.

Stage	Sample	Hg (ppb)	TOC	Al_2O_3	Mo	Hg/TOC	Hg/ Al_2O_3	Height (cm)
	Method	AAS	Eltra CS-500	ICP-ES	ICP-MS			
		ppb	%	%	ppm			
	MDL	0,2		0.01	0.1			
	K 8	16.2	0.79	5.28	0.4	20.5	3.1	408.5
	K 7	6.9	0.68	5.29	0.2	10.1	1.3	353.5
	K 6	11.0	0.19	19.45	0.1	57.9	0.6	308.5
	K 5	5.2	0.67	4.17	0.1	7.8	1.2	263.5
	K 4	8.5	0.65	2.97	0.1	13.1	2.9	243.5
	K 3	9.3	0.72	1.75	0.1	12.9	5.3	231.5
	K 2	18.9	0.59	4.89	0.5	32.0	3.9	223.5
FAMENNIAN	K 1	22.5	0.71	3.81	1.4	31.7	5.9	208.5
FRASNIAN	K 0 CH	2517.3	7.04	17.21	40.8	357.6	146.3	203
Upper KW	K 01 ?CH	93.0	0.64	5.98	2.0	145.3	15.6	201
	K 02	22.7	0.64	5.82	0.2	35.5	3.9	200
	K 03	23.6	0.31	17.09	0.5	76.1	1.4	185
Inter KW	K 05	10.6	0.70	3.29	0.1	15.1	3.2	145
	K 06	36.4	0.59	5.42	0.1	61.7	6.7	95
	K 07 ?Sx	63.3	0.43	15.49	0.1	147.2	4.1	55
	K 08	42.1	0.82	1.52	0.1	51.3	27.7	23
Median value		**20.7**	0.66	5.29	0.15	32.0	3.9	
Spearman’s rs correlation coefficient		Hg	0.05	0.44	0.44			

?Volcaniclastics

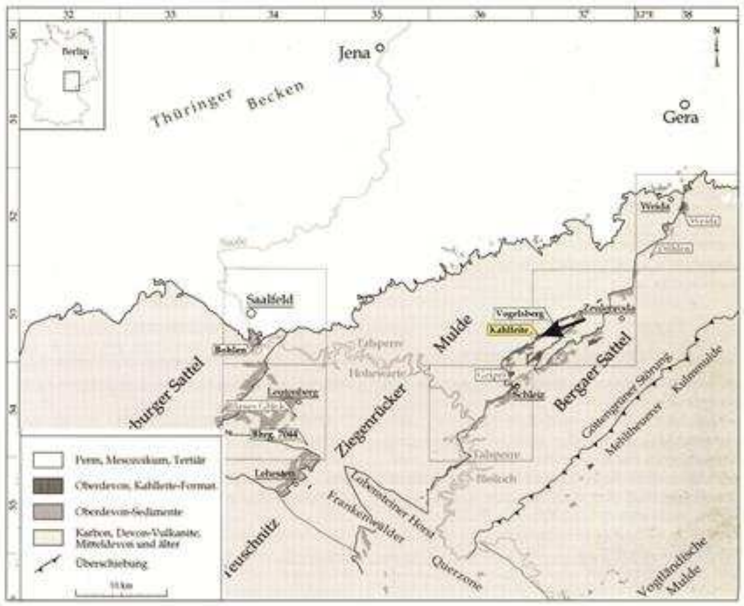

S 3. Location of Kahlleite section (arrowed) in central Germany (from Gereke, 2007).

S 4. General view of the quarry wall exposing the upper Frasnian and the F-F boundary interval (left), and close-up of the F-F boundary beds at Kahlleite (September 2012; right).

3. Syv'yu, Subpolar Urals, north-eastern European Russia

Coordinates: 65°45'58.2" N; 59°30'30.8" E

The geology and geochemistry of the deep-slope succession of the Timan–Pechora Basin, West–Urals structural zone, was studied in detail by Yudina et al. (2002). The Syv'yu River section is located in the vicinity of the town of Inta (Subpolar Urals) near Vorkuta (Komi Republic), about 38 km up-stream from its junction with the Kozhym River. The Upper Devonian deposits, exposed along the right bank of Syv'yu River in several outcrops, represent an almost continuous sequence of the clayey-siliceous-carbonate (Domanic–type) deposits through the Frasnian and lower Famennian, and comprise thinly bedded, westerly dipping strata, without tectonic complications. For present paper, 62 archival samples, from a densely sampled 7.8 m interval, yielded in 1999 by Alexandra Yudina, were re-measured.

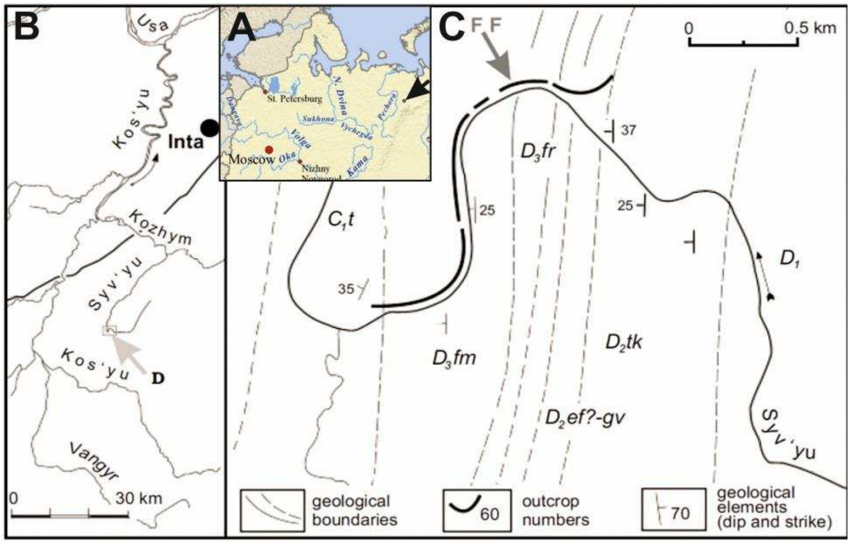

S 5. Location of Syv'yu locality in northern European Russia (A), Kozhym River basin (B), and locality map of studied outcrops along the Syv'yu River section, western slopes of the Subpolar Urals (C); C1t, Tournaisian. D1, Lower Devonian; D2tk, ?Middle Devonian, Takata Suite; D2ef–gv, Eifelian–Givetian; D3fr, Frasnian; D3fm, Famennian (from Yudina et al., 2002, fig. 1).

Hg, Al_2O_3, Mo contents, and Hg/TOC and Hg/Al_2O_3 ratios from F-F succession of Syv'yu River.

Stage	Sample	**Hg**	**TOC**	**Al_2O_3**	**Mo**	**Hg/ TOC**	**Hg/ Al_2O_3**	**Height (cm)**
	Method	AAS	Eltra CS-500	ICP-ES	INAA			
		ppb	%	%	ppm			
	MDL	0.2	0.01	0.01	2 or 5			
	SYV 96 - S10	21.8	2.24	no data	no data	9.8	x	775
	SYV 96 - S12	23.2	1.64	no data	no data	14.1	x	748,5
	SYV 96 - S 9	21.8	2.19	no data	no data	10.1	x	739,5
	SYV 96 - S7	16.4	1.46	no data	no data	11.0	x	714,5
	SYV 96 - S4	15.3	2.79	no data	no data	5.4	x	651,5
	SYV 96 - 134A	12.9	1.89	0.21	<5	6.9	61.5	613,5
	SYV 96 - 132	23.5	3.09	no data	no data	7.5	x	599
	CB 99355	24.2	1.39	0.33	<5	17.2	73.4	591
	CB 99354	36.8	1.40	0.34	<5	26.5	108.2	585,5
	CB 99353	26.6	1.64	0.43	<5	27.4	104.5	582,5
	CB 99352	43.0	2.04	0.48	<5	21.1	89.6	581,5
	CB 99351	44.9	2.40	0.63	<5	19.6	74.9	578
	CB 99350	47.2	2.0	0.87	<5	23.57	54.3	575,5
	CB 99349	33.8	2.00	0.39	<5	17.0	86.5	573,5
Famennian	SYV 96 - 138/1	26.9	2.13	0.27	<5	12.7	99.8	571,5

Frasnian	CB 99348	50.5	2.66	0.24	<5	19.2	210.4	570,5
	CB 99347* ” CH	120.8	1.33	0.19	<2	90.9	636.8	568,5
	CB 99346	109.8	2.11	0.30	<5	52.2	366.0	566,5
	CB 99345” ?CH	109.6	1.65	0.07	<2	66.5	1571.4	564,5
	CB 99344	89.9	2.47	0.15	<5	36.5	599.3	561,5
	CB 99342	65.4	1.97	0.22	<5	33.1	297.4	556,5
	CB 99341	39.7	3.00	0.45	<5	13.3	88.2	555,5
	CB 99340	153.6	3.05	0.68	<5	50.5	225.9	554,5
	CB 99339 ?	162.2	2.41	0.56	<5	67.3	289.6	553,5
	CB 99338	111.2	2.65	0.55	6	42.0	202.1	552,5
	CB 99337 ?	237.0	2.10	1.09	<5	112.9	217.4	550,5
	CB 99336 ?	260.5	2.32	0.44	<5	112.2	591.9	549,5
	CB 99335	41.6	2.17	0.54	<5	19.3	77.1	546,5
	CB 99334	93.5	4.18	1.26	<5	22.2	74.2	543,5
Upper KW	CB 99333	132.6	3.71	1.09	<5	35.9	121.7	542
	CB 99332	42.8	3.48	1.14	<5	12.3	37.5	539,5
	CB 99331	42.2	4.05	1.13	<5	10.4	37.3	537
	CB 99330	24.5	3.35	0.54	<5	7.2	45.3	535
	CB 99329	23.8	3.00	0.38	<5	8.0	62.7	531,5
	CB 99328	36.7	3.13	0.36	<5	11.8	101.9	526,5
	CB 99327 ?	233.9	2.81	0.98	25	83.3	238.6	523,5
	CB 99326	41.3	2.58	1.15	<5	15.9	35.9	521,5
	CB 99325	191.6	5.54	9.66	17	34.7	19.8	513
	CB 99323	96.4	2.37	6.24	8	40.6	15.4	502
	CB 99322	59.5	2.73	6.75	<5	22.0	8.8	495,5
	CB 99321	49.5	3.12	5.71	<5	15.7	8.7	492
	CB 99320	107.5	2.09	10.99	<5	51.1	9.8	481,5
	CB 99318 ?Sx	212.6	2.84	1.95	<5	74.9	109.0	458,5
	CB 99317	61.5	1.36	2.09	<5	45.6	29.4	451,5
	CB 99316 ?Sx	221.5	1.84	10.92	<5	120.0	20.3	443
	CB 99314	109.2	2.08	11.23	<5	52.4	9.7	427,5
	CB 99313	36.7	2.24	2.18	<5	16.6	16.9	419
	CB 99312	59.5	1.16	13.75	<5	51.0	4.3	415,5
	CB 99310	25.1	1.81	1.49	<5	13.8	16.9	399
	CB 99309	94.1	2.11	7.66	<5	44.6	12.3	391
	CB 99305	25.4	1.55	2.02	<5	16.1	12.6	351,5
Inter KW	CB 99301	32.9	1.38	2.57	<5	23.9	12.8	305,5
	CB 99300	46.1	0.62	15.79	<5	74.2	2.9	297,5
	CB 99229	18.5	1.75	1.64	<5	10.3	11.3	295
	CB 99228	36.4	1.90	1.80	<5	18.9	20.2	288
	CB 99227	51.7	2.28	7.04	<5	22.8	7.3	282,5
	CB 99226	16.4	1.83	1.11	<5	8.8	14.8	275
	SYV 96 - 100	37.3	1.84	1.18	<5	20.1	31.6	220
	SYV 96 - 91	17.1	2.92	no data	no data	5.8	x	67
	CB 99222	36.4	0.83	0.49	<5	43.2	74.3	0
	CB 9921	37.0	1.27	no data	no data	29.1	x	Omitted in Fig.
	SYV 96 – 64	18.7	1.62	no data	no data	11.7	x	
Median value		**42.5**	2.17	1.14	x	21.5	62.7	
Spearman’s rs correlation		Hg	0.23	017	x			

*Samples analyzed in more refined variant

[pink box] Zr enrichment (up to eightfold) and probable volcaniclastic admixture (Na−feldspars, micas, illite–smectite mixed layer clays, amorphous particles of ?glass shards; Yudina et al., 2002, fig. 7)

(DR 3) ANALYTHICAL METHODS

Mercury determination

Bulk samples from Lahmida and Kahlleite sections were first analyzed geochemically for trace elements at the Bureau Veritas AcmeLabs, Vancouver, Canada. Hg concentrations were determined using the ICP-MS method and precision and accuracy of the results were better than ±10 ppb. Several anomalously high Hg values were established in the measured samples. The Russian samples were originally analyzed for Hg contents by INAA at the Activation Laboratories, Ontario, Canada, by Yudina et al. (2002); single samples, however, yield values below the method detection level (1000 ppb).

Subsequently, Hg determination of 122 samples from all three sections was refined using atomic absorption spectrometry (AAS) Milestone DMA-80 Direct Mercury Analyzer (http://www.milestonesrl.com/landing-page/dma-80/) in the Faculty of Earth Sciences, University of Silesia (Poland). This commonly used analyzer assess samples by thermal decomposition, Hg amalgamation and atomic absorption detection, and has a detection limit of 0.2 ppb. The DMA analytical curves were prepared with dilution of a 1 mg L-1 standard solution (Merck Darmstadt, Germany). Measurement of each sample was duplicate and analyses were repeated when the coefficient of variability of samples exceeds 5%. The instrument was calibrated using certified reference material INCT-OBTL-5 (tobacco leaves) prior to the measurement, with Hg content = 20.9 ppm. The measured error did not exceed 2%. In another Hg study, with use of the same analyzer type, accuracy and precision of the determinations was estimated as ca. 8 and 6.5%, respectively (Sabatino et al., 2018).

Total organic carbon (TOC)

Total carbon (TC) contents were determined using an Eltra CS-500 IR-analyzer with a TIC (total inorganic carbon) module. TC was determined using an infrared cell detector. TIC content was determined by infrared detector as carbon dioxide derived from carbonates reacted with 15% warm hydrochloric acid. TOC was calculated as the difference between TC and TIC. Instrument calibration used Eltra standards. Analysis were performed in Faculty of Earth Sciences, University of Silesia (Poland).

Aluminum and molybdenum determinations

Al and Mo concentrations (DR 2) were analyzed at Bureau Veritas AcmeLabs, Vancouver, Canada, with the exception of samples from Russia, which were analyzed at Activation Laboratories, Ontario, Canada (Yudina et al., 2002). Al content was determined using ICP-ES method and precision and accuracy of the results were better than 0.01 %. Mo concentration was determined by ICP-MS method (detection level = 0.01 ppm; Lahmida, Kahlleite) or in two analytical variants by INAA (detection level = 2 or 5 ppm; Syv'yu).

(DR 3) THE STRONGEST HG AND HG/TOC SIGNALS OF THE "BIG FIVE" MASS EXTINCTIONS

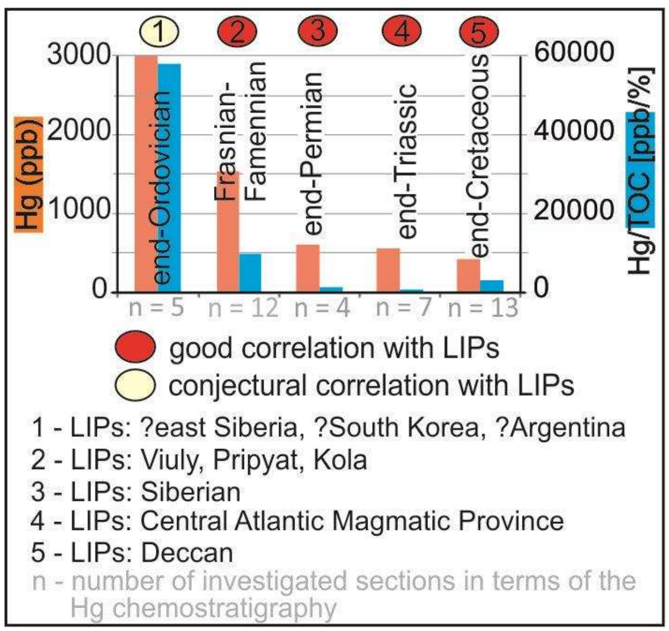

K-P: Nascimento Silva et al. (2011, 2013), Sial et al. (2013, 2014, 2016), Font et al. (2016)

J-T: Thibodeau et al. (2016), Precival et al. (2017)

P-T: Sanei et al. (2012), Grasby et al. (2013, 2015, 2017)

O-S: Jones et al. (2017), Gong et al. (2017)

REFERENCES CITED:

Dopieralska, J., 2003, Neodymium isotopic composition of conodonts as a palaeoceanographic proxy in the Variscan oceanic system: Ph.D. Thesis, Justus-Liebig-University, Giessen, 111 p.

Dopieralska, J., 2009, Reconstructing seawater circulation on the Moroccan shelf of Gondwana during the Late Devonian: Evidence from Nd isotope composition of conodonts: Geochemistry, Geophysics, Geosystems, v. 10 (3). p. 1-10, doi: 10.1029/2008GC002247.

Font, E., Adatte, T., Sial, A.N., de Lacerda, L.D., Keller, G., and Punekar, J., 2016, Mercury anomaly, Deccan volcanism, and the end-Cretaceous mass extinction: Geology, v. 44, p. 171–174, doi: 10 .1130 /G37451 .1.

Gereke, M., 2004, Das Profil Kahlleite Ost - die stratigraphische Entwicklung einer Tiefschwelle im Oberdevon des Bergaer Sattels (Thüringen). Geologica et Palaeontologica 38, 1–31.

Gereke, M., 2007, Die oberdevonische Kellwasser-Krise in der Beckenfazies von Rhenoherzynikum und Saxothuringikum (spätes Frasnium/frühestes Famennium, Deutschland). Kölner Forum für Geologie und Paläontologie 17, 1–228.

Gereke, M., and Schindler, E., 2012, "Time-Specific Facies" and biological crises — The Kellwasser Event interval near the Frasnian/Famennian boundary (Late Devonian): Palaeogeography, Palaeoclimatology, Palaeoecology, v. 367–368, p. 19–29, doi: 10.1016/j.palaeo.2011.11.024.

Gong, Q., Wang, X., Zhao, L., Grasby, S.E., Chen, Z-Q., Zhang, L., Li, Y., Cao, L., and Li, Z., 2017, Mercury spikes suggest volcanic driver of the Ordovician-Silurian mass extinction: Scientific Reports, 7, p. 1-7, doi: 10.1038/S41598-017-05524-5.

Grasby, S.E., Sanei, H., Beauchamp, B., and Chen, Z., 2013, Mercury deposition through the Permo- Triassic biotic crisis: Chemical Geology, v. 351, p. 209–216, doi: 10 .1016 /j .chemgeo .2013 .05 .022.

Grasby, S.E., Beauchamp, B., Bond, D.P.G., Wignall, P.B., and Sanei, H., 2015, Mercury anomalies associated with three extinction events (Capitanian crisis, latest Permian extinction and the Smithian/Spathian extinction) in NW Pangea: Geological Magazine, v. 153, p. 285–297, doi: 10 .1017 /S0016756815000436.

Grasby, S.E., Shen, W., Yin, R., Gleason, J.D., Blum, J.D., Lepak, R.F., Hurley, J.P., Beauchamp, B., 2017, Isotopic signatures of mercury contamination in latest Permian oceans: Geology, v. 45, p. 55-58, doi:10.1130/G38487.1 |

Hammer, Ø., 1999-2009, PAST PAleontological Statistics Version 1.94b. Reference manual: Natural History Museum, University of Oslo, 175 p.

Jones, D.S., Martini, A.M., Fike, D.A., and Kaiho, K., 2017, A volcanic trigger for the Late Ordovician mass extinction? Mercury data from south China and Laurentia: Geology, v. 45, p. 631-634, doi:10.1130/G38940.1.

Nascimento-Silva, M.V., Sial, A.N., Ferreira, V.P., Neumann, V.H., Barbosa, J.A., Pimentel, M.M., and de Lacerda, L.D., 2011, Cretaceous-Paleogene transition at the Paraíba Basin, Northeastern, Brazil: Carbon-isotope and mercury subsurface stratigraphies: Journal of South American Earth Sciences, v. 32, p. 379–392, doi: 10.1016/j.jsames.2011.02.014.

Nascimento-Silva, M.V., Sial, A.N., Barbosa, J.A., Ferreira, V.P., Neumann, V.H., and de Lacerda, L.D., 2013, Carbon isotopes, rare-earth elements and mercury geochemistry across the K -T transition of the Paraíba Basin, northeastern Brazil, in Bojar, A.V., Melinte-Dobrinescu, M.C., and Smit, J., eds., Isotopic Studies in Cretaceous Research: Geological Society (London) Special Publications 382, p. 85-104, doi: 10.1144/SP382.2.

Percival, L.M.E., Ruhla, M., Hesselbo, S.P., Jenkyns, H.C., Mather, T.A., and Whiteside J.H., 2017, Mercury evidence for pulsed volcanism during the end-Triassic mass extinction: Proceedings of the National Academy of Sciences of the United States of America, v. 114, p. 7929–7934, doi: 10.1073/pnas.1705378114.

Racki, G., 2005, Toward understanding Late Devonian global events: Few answers, many questions, in Over. D.J., Morrow, J.R., and Wignall, P.B., eds., Understanding Late Devonian and Permian–Triassic Biotic and Climatic Events: Towards an Integrated Approach, Developments in Palaeontology and Stratigraphy 20, p. 5–36.

Riboulleau, A., Spina, A., Vecoli, M., Riquier, L., Quijada, M., Tribovillard, N., and Averbuch, O., 2018, Organic matter deposition in the Ghadames Basin (Libya) during the Late Devonian: a multidisciplinary approach. Palaeogeography, Palaeoclimatology, Palaeoecology, doi: 10.1016/j.palaeo.2018.02.004.

Sabatino, N., Ferraro, S., Coccioni, R., Bonsignore M., Del Core, M., Tancredi, V., Sprovieri, M., 2018. Mercury anomalies in upper Aptian-lower Albian sediments from the Tethys realm. Palaeogeography, Palaeoclimatology, Palaeoecology 495, 163-170.

Sanei, H., Grasby, S.E., and Beauchamp, B., 2012, Latest Permian mercury anomalies: Geology, v. 40, p. 63–66, doi:10.1130/G32596.1

Sial, A.N., Lacerda, L.D., Ferreira, V.P., Frei, R., Marquillas, R.A., Barbosa, J.A., Gaucher, C., Windmöller, C.C., and Pereira, N.S., 2013, Mercury as a proxy for volcanic activity during extreme environmental turnover: the Cretaceous–Paleogene transition: Palaeogeography, Palaeoclimatology, Palaeoecology, v. 387, p. 153–164, doi: 10.1016/j.palaeo.2013.07.019.

Sial, A.N., Chen, J.-B., Lacerda, L.D., Peralta, S., Gaucher, C., Frei, R., Cirilli, S., Ferreira, V.P., Marquillas, R.A., Barbosa, J.A., Pereira, N.S., and Belmino, I.K.C., 2014, High-resolution Hg chemostratigraphy: A contribution to the distinction of chemical fingerprints of the Deccan volcanism and Cretaceous–Paleogene boundary impact event. Palaeogeography, Palaeoclimatology, Palaeoecology, v. 414, p. 98–115, doi: 10.1016/j.palaeo.2014.08.013.

Sial, A.N., Chen, J., Lacerda, L.D., Frei, R., Tewari, V.C., Pandit, M.K., Gaucher, C., Ferreira, V.P., Cirilli, S., Peralta, S., Korte, C., Barbosa, J.A., and Pereira, N.S., 2016, Mercury enrichment and Hg isotopes in Cretaceous–Paleogene boundary successions: Links to volcanism and palaeoenvironmental impacts: Cretaceous Research, v. 66, p. 60–81, doi: 10.1016/j.cretres.2016.05.006.

Thibodeau, A.M., Ritterbush, K., Yager, J.A., West, A.J., Ibarra, Y., Bottjer, D.J., Berelson, W.M., Bergquist, B.A., and Corsetti, F.A., 2016, Mercury anomalies and the timing of biotic recovery following the end-Triassic mass extinction: Nature Communications, v. 7, p. 1-8, doi: 10 .1038 /ncomms11147.

Wendt, J., and Belka, Z., 1991, Age and depositional environment of Upper Devonian (Early Frasnian to Early Famennian) black shales and limestones (Kellwasser Facies) in the Eastern Anti-Atlas. Morocco: Facies, v. 25, p. 51-90, doi: 10.1007/BF02536755.

Yudina, A.B, Racki, G., Savage, N.S., Racka, M., and Małkowski, K., 2002, The Frasnian-Famennian events in a deep-shelf succession, Subpolar Urals: Biotic, depositional and geochemical records: Acta Palaeontologica Polonica, v. 47, p. 355-372.